

Evidence for Two Separate One-Electron Transfer Events in Excited Fulleropyrrolidine Dyads Containing Tetrathiafulvalene (TTF)

Nazario Martín,* Luis Sánchez, and M^a Angeles Herranz

Departamento de Química Orgánica I, Facultad de Química, Universidad Complutense, E-28040 Madrid, Spain

Dirk M. Guldi*

Radiation Laboratory, University of Notre Dame, South Bend, Indiana

Received: November 22, 1999; In Final Form: February 22, 2000

1,3-Dipolar cycloadditions of TTF-azomethine ylides (TTF = tetrathiafulvalene) to C₆₀ have been used to synthesize a series of novel donor–bridge–acceptor dyads. In these dyads the pyrrolidine[3',4':1,2][60]fullerene is covalently attached to the electron donor TTF either directly (**5**) or alternatively through one (**2a**) or two (**7**) vinyl groups. In the ground state, dyads **2a**, **5**, and **7** undergo four quasireversible one-electron reductions and two reversible oxidation steps. The former are associated with the reduction of the C₆₀ core, whereas the latter correspond to the formation of the radical cation and dication of the TTF moiety, respectively. Semiempirical PM3 calculations reveal donor–acceptor distances of 4.8 Å (**5**), 7.6 Å (**2a**), and 10.5 Å (**7**), and a deviation from planarity between the TTF fragment and the vinylogous spacer. In relation to an *N*-methylfulleropyrrolidine, the emission of the fullerene singlet excited state in dyads **2a**, **5**, and **7** is substantially reduced. Furthermore, the fluorescence quantum yield correlates well with the solvent dielectric constant and also with the spatial separation of the donor and acceptor moieties in the dyads. These correlation suggest that intramolecular electron-transfer processes evolving from the fullerene singlet excited state generate the (C₆₀^{•-})–(TTF^{•+}) pair. Pico- and nanosecond-resolved transient spectroscopy further substantiate a rapid transformation of the initially formed singlet excited state into the charge-separated radical pair with intramolecular rates ranging between $1.17 \times 10^{10} \text{ s}^{-1}$ and $1.47 \times 10^9 \text{ s}^{-1}$. In all cases, the product of back electron transfer is the triplet excited state, which is generated with markedly high quantum yields (0.61–0.97). The latter is, in addition to the rapid primary intramolecular electron transfer, subject to a slower, secondary intermolecular electron transfer with rate constants of $7 \times 10^8 \text{ M}^{-1}\text{s}^{-1}$ (**5**) in benzonitrile and $1.6 \times 10^9 \text{ M}^{-1} \text{ s}^{-1}$ (**5**) in toluene.

Introduction

The rational design of molecules capable of achieving photoinduced charge separation with a high quantum efficiency has been an important task in chemistry for the last years.^{1–5} The advent of fullerenes^{6,7} as promising electroactive chromophores opened up a new approach to this goal. The redox properties of the ground and excited states of [60]fullerene have been used for the design of devices with complex functions, such as artificial photosynthetic systems and photoactive dyads. This work evoked a lively interest to study fullerenes with regard to efficient charge separation.⁸ Furthermore, the combination of a spherical symmetry, strong pyramidalization of the individual carbon atoms,⁹ and the low reorganization energy of the carbon network,¹⁰ renders [60]fullerenes unique candidates for building blocks of more complex systems. As a consequence, a wide variety of electron-donor units have been covalently attached to the C₆₀ framework in recent years.¹¹

Among the various methodologies that enable the linkage of a broad spectrum of donor moieties to C₆₀, cycloaddition reactions play an outstanding role.¹² Specifically, Diels–Alder and 1,3-dipolar cycloadditions are particularly successful.¹³ Alternatively, the Bingel's reaction¹⁴ [e.g., addition of bis-(ethoxycarbonyl)methylene groups] proved to be another good concept for the design and preparation of dyads in which the

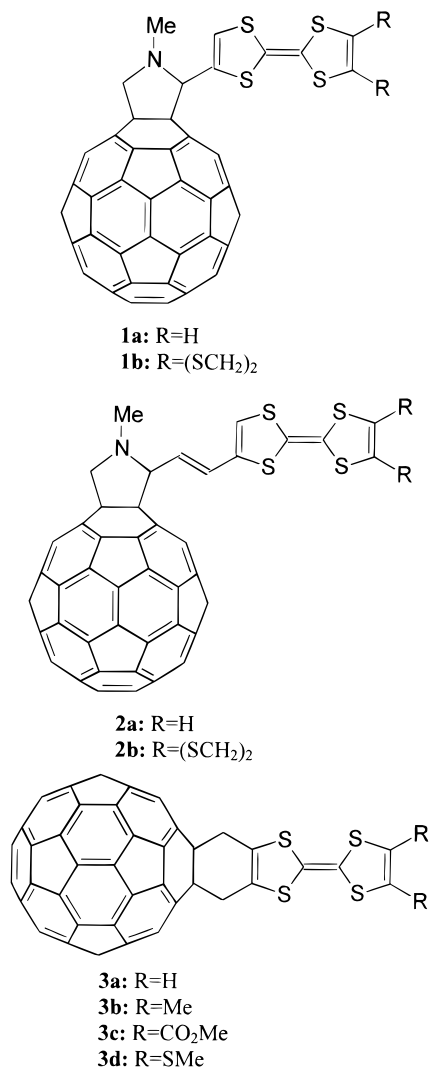
pendant fullerene acts as an electron-acceptor component. By following these synthetic approaches, different donor fragments have been attached to C₆₀ to form C₆₀-based dyads and triads.¹¹

Tetrathiafulvalenes (TTFs) are remarkable with respect to their involvement in redox reactions. In their one-electron oxidized form (namely, the 1,3-dithiolium cation), they display a $(4n + 2)$ aromatic character, in contrast to the ground state. In view of electron-transfer processes, this gain of aromaticity is an important requisite, assisting in the stabilization of charge-separated radical pairs. Additionally, TTF and its derivatives undergo two one-electron oxidation steps at well-defined redox potentials to form the corresponding radical cations and dications. The latter have been successfully employed as starting materials for the preparation of electrically conducting and superconducting TTF salts and TTF charge-transfer complexes.¹⁵

The systematic functionalization of TTF is a very active research field of interdisciplinary interest. For example, **6**¹⁶ was prepared in a one-pot synthesis involving monolithio-TTF and 5-(*N,N*-diethylamino)-4-pentadienal¹⁷ by following Jutz's procedure.¹⁸ The latter concept has been extended to other organolithium systems by Friedly et al.¹⁹

We have recently reported the synthesis of TTF-containing organofullerenes **1** and **2**, via a 1,3-dipolar cycloaddition of azomethine ylides to C₆₀ starting from a formyl-TTF precursor.²⁰

CHART 1



In these compounds, the TTF unit is either directly linked to the fullerene pyrrolidine ring²¹ (**1a,b**) or through an ethylene spacer (**2a,b**) (Chart 1). In the solid state, **1a** and **2a** form charge-transfer (CT) complexes with strong electron-acceptors, such as 2,3,5,6-tetrafluor-7,7,8,8-tetracyano-*p*-quinodimethane (TCNQF₄), which at a 1:1 donor:acceptor stoichiometry display semiconducting behavior.²⁰

The C₆₀-TTF donor-bridge-acceptor dyads of type **3** have been prepared by Diels-Alder cycloaddition of the respective *o*-quinodimethane analogues of TTF and [60]fullerene.²² The cationic and anionic species of compounds **3a-c** give rise to electron paramagnetic resonance (EPR) signals and ³²S hyperfine coupling constants that reveal spin density distributions located on the TTF and [60]fullerene moieties, respectively.²³ In nanosecond-resolved flash photolysis, these systems undergo a rapid quenching of the triplet excited states generating, in the case of **3a** and **3b**, transient charge-separated open-shell species with lifetimes typically around 75 μs.²³ No information is given, however, with respect to the potential participation of the fullerene singlet excited state in intramolecular electron transfer processes. The scope of our current study is to apply a time resolution of a few tens of picoseconds, to monitor the entire dynamic range and to optimize the charge separation via a controlled separation of the donor-acceptor moieties.

The nature and length of the spacer connecting both donor and acceptor moieties exert a profound impact on the rate and

efficiency of intramolecular electron-transfer processes.²⁴ In this paper we report on the synthesis, electrochemistry, and photo-physical properties of novel C₆₀-TTF dyads **5** and **7**, in addition to the previously synthesized organofullerene **2a**.²⁰ In these compounds, the TTF donor unit is attached to the fulleropyrrolidine moiety through a single σ -bond (**5**) and one (**2a**) or two (**7**) vinyl spacers. In this context, effects will be elucidated that show the influence of both the distance between donor and acceptor moieties and the solvent polarity on intramolecular dynamics and the efficiency of charge separation.

Most of the reported fullerene-donor dyads (e.g., ferrocene and aniline) display a back electron-transfer process following photoinduced electron transfer that leads to a direct regeneration of the singlet ground state. This process can be rationalized in terms of the oxidation potentials of the ferrocene and aniline donor moieties, which consequently move the energies of the charge-separated states [(C₆₀^{•-})-(Fc^{•+}) and (C₆₀^{•-})-(aniline^{•+})] well below that of the fullerene triplet state. It will be shown that in TTF-containing dyads **2a**, **5**, and **7**, the triplet excited state is actually the result of back electron-transfer. The high quantum yield of the triplet excited state is beneficial by enabling a slower, secondary intermolecular electron transfer in addition to the rapid primary intramolecular electron transfer.

Results and Discussion

Synthesis. Target molecules **5** and **7** were prepared via 1,3-dipolar cycloaddition of azomethine ylides to C₆₀.²⁵ Accordingly, the *N*-unsubstituted dyad **5** was obtained, in moderate yield (30% yield, 48% yield based on reacted C₆₀), through a reaction of formyltetraathiafulvalene (**4**)²⁶ with glycine and [60]fullerene. Similarly, dyad **7** was synthesized (27% yield, 53% yield based on reacted C₆₀) by reacting the formyl-containing TTF derivative **6** with sarcosine (*N*-methylglycine) and [60]fullerene.

Formyl-containing TTFs are usually prepared by lithiation of TTF and further reaction with the formylating reagent. Preparation of formyl-TTF vinylogues requires a subsequent Wittig reaction of formyl-TTF with phosphoranes. Recently, we have developed a facile one-pot synthesis of formyl-TTF vinylogues (such as **6**) in satisfactory yields from monolithio-TTF and commercially available, or easily synthesized, unsaturated *N,N*-dimethylaminoaldehydes.¹⁶

The structures of **5** and **7** were characterized by ultraviolet-visible (UV-vis), Fourier transform infrared (FTIR), proton and carbon-13 nuclear magnetic resonance (¹H and ¹³C NMR, respectively) and fast-atom bombardment (FAB) spectroscopy. Specifically, the ¹H NMR spectrum of **5** reveals a pyrrolidine proton doublet at δ 5.01 and δ 4.77 ($J = 10.2$ Hz, geminal hydrogens) followed by a singlet at 5.63 (CH), whereas **7** shows a doublet at δ 4.85 and δ 4.12 ($J = 9.3$ Hz) and a doublet at δ 4.38 (CH, $J = 8.7$ Hz).

The ¹³C NMR spectra of dyads **5** and **7** show that although the resonances observed were less than expected due to the superposition of several signals, the number of resonances reveals the lack of symmetry in these compounds. In addition to the N-Me group of **7**, which appears at 40.1 ppm, there are signals for the *sp*³ carbons of the pyrrolidine ring and for the 6,6-junction of the C₆₀ framework. The latter appear at 77.2, 72.7, 71.4, and 61.0 ppm (for **5**) and 81.8, 77.2, 69.7, and 69.3 ppm (for **7**), which is in good agreement with other *N*-methyl fulleropyrrolidine derivatives.²⁵

The positive liquid secondary ion mass spectra (LSIMS) in 3-nitrobenzyl alcohol (NBA) matrix showed the molecular ions for **5** and **7** at m/z 965 and 1031, respectively.

TABLE 1: Redox Properties of Fullerene–TTF Dyads **2a, **5** and **7**^a**

compound	$E^1_{1/2ox}$	$E^2_{1/2ox}$	E^1_{red}	E^2_{red}	E^3_{red}	E^4_{red}
5	0.51	0.87	-0.65	-1.08	-1.65	-2.12
2a	0.43	0.76	-0.67	-1.08	-1.58	-2.19
7	0.48	0.83	-0.66	-1.04	-1.65	-2.17
TTF	0.37	0.70				
C ₆₀			-0.60	-1.00	-1.52	-2.04

^a All potentials in V versus SCE; Tol:MeCN (4:1) as solvent; scan rate, 200 mV/s; 0.1 mol·dm⁻³ Bu₄N⁺ClO₄⁻ as supporting electrolyte; GCE as working electrode.

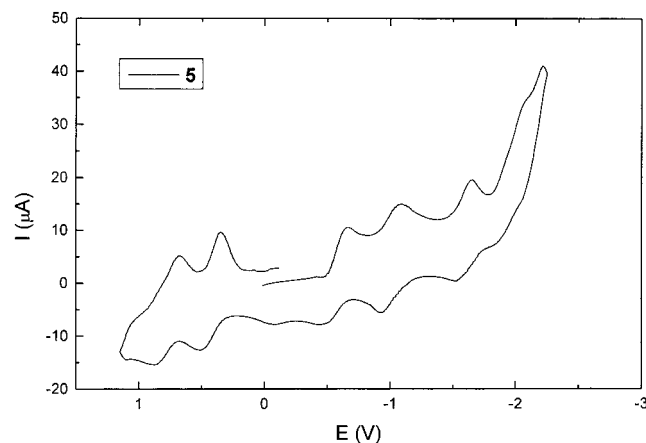


Figure 1. Cyclic voltammetry of fulleropyrrolidine **5** at 200 mV/s in toluene:MeCN (4:1, v/v) at room temperature using Bu₄N⁺ClO₄⁻ as supporting electrolyte.

The UV–vis spectra of **5** and **7** display an absorption band around 430 nm, which is a characteristic signature of [6,6]-closed fullerene derivatives. Accordingly, this signature unmistakably confirms the linkage of the organic TTF-addends at the 6,6-ring junction of the C₆₀ framework.²⁷ In room-temperature solutions, the singlet ground-state spectra of dyads **1** and **2** provide no evidence for a charge-transfer interaction between the two electroactive moieties. In contrast to the condensed phase, solid-state EPR spectra of **1a** (both at room temperature and 5.2 K) give rise to weak signals that were assigned to solid-state interaction.²⁸ Furthermore, these observations resemble those noticed in EPR studies carried out with dyads **3a–c**.²³

Electrochemistry. The electrochemical properties of dyads **2a**, **5**, and **7** have been studied by cyclic voltammetry at room temperature. The corresponding data are collected in Table 1 along with the redox potentials of TTF and the C₆₀ reference.

Dyads **2a**, **5**, and **7** give rise to four quasireversible one-electron reduction waves that reflect the individual reduction steps of their fullerene cores (Figure 1). In general, these reduction potential values are shifted to more negative values, relative to [60]fullerene. This shift stems from the saturation of a double bond in the C₆₀ core that raises the lowest unoccupied molecular orbital (LUMO) energy of the resulting organofullerene accordingly.²⁹ It should be noted that the first reduction potential values for these dyads (**5**, **2a**, and **7**) are all quite similar. The noted resemblance indicates that the presence of the vinylogous spacers between the donor and acceptor moieties has no measurable effect on the electron-accepting properties of the C₆₀ moiety.

On the anodic side, two reversible oxidation waves are observed at positive potentials, corresponding to the radical cation and dication species of the TTF fragment, respectively. Compared with TTF, the oxidation potentials are, however, anodically shifted by ~100 mV. This shift can be rationalized in terms of the substitution effects on the TTF unit.³⁰

In conclusion, the CV measurements confirm that both the donor and acceptor components preserve their individual electroactive identity and that they lack any mutual electronic interaction in the ground state. These findings are in good agreement with the assumption derived from the electronic ground-state spectra as well as from Raman studies on dyads **1a**²¹ and **3a–d**.^{22,23}

PM3-Optimized Structures. Previously, we reported the PM3-optimized structure of dyad **1a** together with the calculated molecular orbital (MO) distribution.²⁸ In dyad **1a**, the highest occupied molecular orbital (HOMO) is localized on the TTF end with essentially the same orbital composition as the parent TTF. In contrast to pristine C₆₀, the three degenerate MOs are split into three different orbitals in dyad **1a**. However, the LUMO is still located on the fullerene framework and lacks any noticeable contribution from the organic addend.²⁸ It is important to note that this molecular distribution remains unchanged in dyads **2a**, **5**, and **7**.

To determine the distance between the TTF donor and the C₆₀ acceptor framework, we calculated the structures of **2a**, **5**, and **7**, in a similar fashion, by semiempirical PM3 geometry minimizations with Hyperchem 5.1.³¹ The optimized geometries of dyads **2a**, **5**, and **7** are shown in Figure 2. The bond numbers between the C₆₀ surface and the closest sulfur atoms are 3, 5, and 7, which leads to through-bond distances of 4.8 Å (**5**), 7.6 Å (**2a**), and 10.5 Å (**7**). In addition, the interchromophore distances from the closest sulfur atom of the TTF moiety to the C₆₀ surface amount to 3.8, 5.2, and 7.2 Å in dyads **5**, **2a**, and **7**, respectively.

Finally, a deviation from planarity of ~30° is noted between the TTF unit and the vinylogous spacers leading to a slightly distorted configuration that has no significant impact on the calculated distances between the two centers. The energy of the latter is lowered by 0.1–0.2 kcal/mol relative to a planar configuration.

Photophysical Measurements. Steady-State Emission Studies: Intramolecular Electron-Transfer Event. The combination of an electron acceptor that exhibits a low reorganization energy and an electron donor that gains aromaticity on oxidation is appealing in light of photoactive materials that are designed for rapid intramolecular electron-transfer processes. A convenient means to probe such electron-transfer events, involving, for example, the fullerene singlet excited state in dyads **2a**, **5** and **7** and a covalently attached electron donor (TTF), is steady-state fluorescence at ambient temperature or in frozen matrixes.

Considering its simplicity, an *N*-methylfulleropyrrolidine was chosen as an internal reference. It is well known that the nitrogen-free lone pair, located at the pyrrolidine ring of this derivative, does not engage in any electron-donating events with the fullerene core. Thus, the noticeably higher fluorescence quantum yield of this fullerene reference ($\Phi = 6.0 \times 10^{-4}$) relative to pristine [60]fullerene ($\Phi = 1.5 \times 10^{-4}$) has been related to the partially broken symmetry of the former.³²

The room-temperature fluorescence (i.e., emission from the singlet excited state) of dyads **2a**, **5**, and **7** (9×10^{-6} M) in toluene solutions, together with the aforementioned fullerene reference, are summarized in Figure 3. In general, the emission spectra of dyads **2a**, **5**, and **7** exhibit structural patterns superimposable on the fullerene reference. Specifically, a strong ⁰0→0 transition at 710 nm is followed by a series of ⁰0→1, ⁰0→2, etc. emissions. These emissions reflect the texture of the (C_{2v}) symmetry of the fullerene core and, more importantly, are virtual mirror images of the singlet ground state absorption bands at 622, 634, 653, 666, 677, 687, and 699 nm. Hereby,

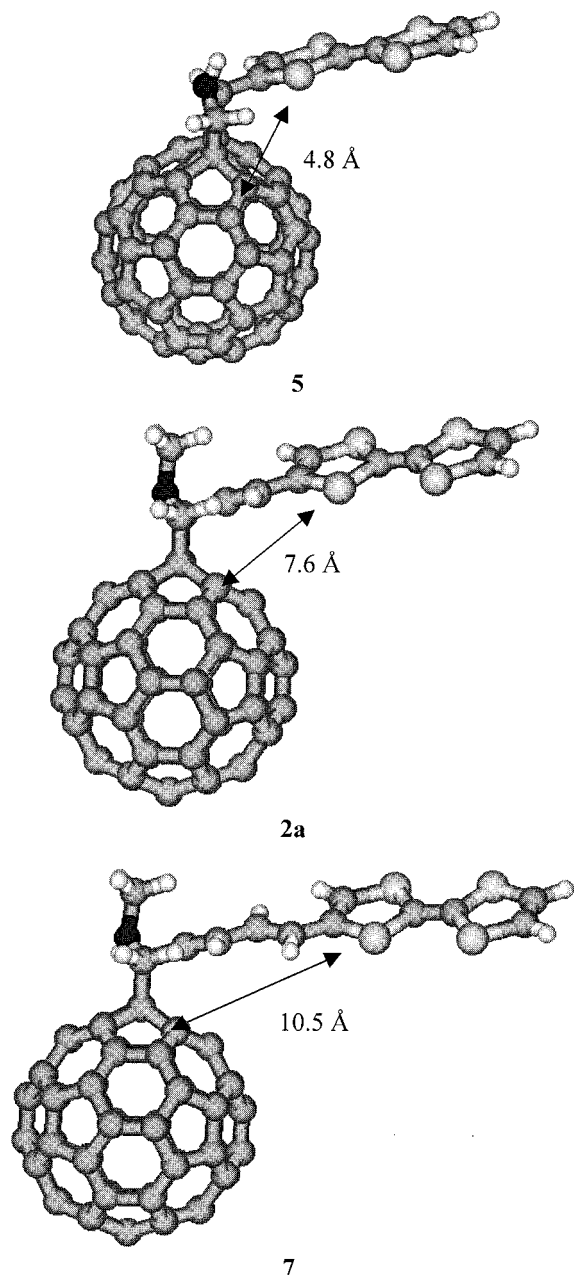
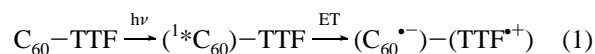


Figure 2. PM3 calculated geometries for dyads **5**, **2a**, and **7**, showing the spatial distances between the TTF and C_{60} chromophores.

the energy of the spectroscopically important $^1S_1 \rightarrow S_0$ transition, which depicts the singlet excited-state energy, is a fundamental parameter for quantifying the envisaged electron-transfer processes (vide infra).

In addition, the similarity of the emission spectra confirms the selective excitation of the fullerene core in dyads **2a**, **5**, and **7**. Under identical scanning conditions, all three dyads give rise to substantially lower emission yields relative to the reference. Considering the moderate oxidation potential of the TTF moiety, which is comparable to electron donors such as ferrocene and aniline,³² we tentatively ascribe the observed emission quenching to the following photoinduced electron-transfer (ET) event:



On the other hand, the lowest singlet excited state of TTF (2.8 eV) is higher than the lowest excited state of the fullerene

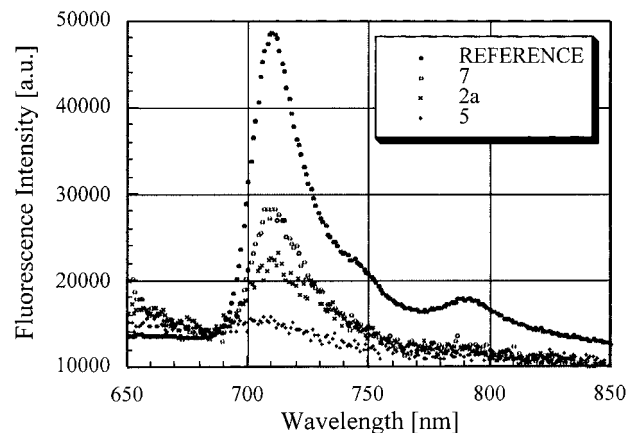


Figure 3. Fluorescence spectra ($\tau_{exc} = 398$ ns) of *N*-methylfulleropyrrolidine (\bullet) and dyads **7** (\circ), **2a** (\times), and **5** ($+$) in toluene solutions (9×10^{-6} M) at room temperature.

(1.76 eV), which rules out an alternative singlet energy transfer mechanism from the singlet excited fullerene state to the TTF moiety.

It is interesting to note that the fluorescence intensities of dyads **2a**, **5**, and **7** reveal a good correlation with their spacer length; that is, the spatial separations between the electron-acceptor (fullerene) and electron-donor moiety (TTF) of 4.8 Å (**2a**), 7.6 Å (**5**), and 10.5 Å (**7**).


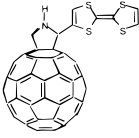
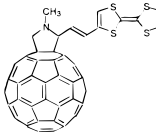
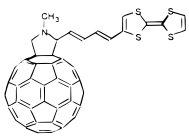
The dielectric continuum model helps to quantify intramolecular electron-transfer processes and in essence predicts a strong impact of the solvent polarity on the redox potential of the donor-acceptor couple and thus on the free energy change of the reaction ($-\Delta G^\circ$).³³ In particular, the exothermicity is expected to increase with the solvent dielectric constant. Thus, in the current context, the fluorescence quantum yields of dyads **2a**, **5**, and **7** were compared in methylcyclohexane, toluene, dichloromethane, and benzonitrile solutions with dielectric constants of 2.02, 2.38, 9.81, and 25.9, respectively. Corresponding experiments in these solvents engenders the expected trend; namely, the stepwise increase of the quenching efficiency on progressing solvent polarity (Table 2). This result clearly supports an intramolecular electron-transfer mechanism (eq 1).

Table 2 lists the calculated ($-\Delta G^\circ$) values for the electron-transfer evolving from the fullerene singlet excited state. In general, a good correlation between the ($-\Delta G^\circ$) values and the quantum yields is noted. From the quantum yields (Φ) of the fluorescence and the lifetime (τ) of the fullerene reference (*N*-methylfulleropyrrolidine; see Table 2), we are able to extract the singlet lifetimes ($\tau_{SINGLET}$) and the rate constants (k_{ET}) of the corresponding electron-transfer reaction of dyads **2a**, **5**, and **7** according to the following expression (see Table 2):⁴

$$k_{ET} = [\Phi(\text{ref}) - \Phi(x)] / [\tau(\text{ref}) \Phi(x)] + k_{ISC} \quad (2)$$

A closer look reveals that the calculated thermodynamic driving force ($-\Delta G^\circ$) and the measured singlet lifetimes of the two vinyl-linked dyads **2a** and **7** do not follow exactly the trend noticed for the directly linked dyad **5**. In this context, and for the sake of simplicity, it is important to note that the calculations just presented have been based on the spatial distance between the two redox active moieties (therefore, any difference in electronic coupling is neglected). Accordingly, a possible rationale for the difference in the deactivation of the singlet excited states of **2a** and **7** stems from the deviation from planarity between the TTF unit and the vinylogous spacers of

TABLE 2: Photophysical Parameters of Fullerene Reference and Fullerene–TTF Dyads 2a, 5 and 7

solvent	parameter				
toluene	$(\Delta G^\circ)_{\text{ET Intra}}^a$		−0.512 eV	−0.179 eV	−0.008 eV
	$\Phi_{\text{FLUORESCENCE}}$	6.0×10^{-4}	0.36×10^{-4}	1.6×10^{-4}	2.58×10^{-4}
	$k_{\text{ET}} [\text{s}^{-1}]^b$		9.1×10^9	1.6×10^9	7.7×10^8
	τ_{SINGLET}		129 ps	395 ps	680 ps
	$k_{\text{ET}} [\text{s}^{-1}]^c$	3.45×10^{8f}	7.8×10^9	2.5×10^9	1.5×10^9
	$k_{\text{BET}} [\text{s}^{-1}]^c$		not resolved	not resolved	not resolved
CH_2Cl_2	Φ_{TRIPLET}^c	0.96	0.96	0.97	0.96
	$(\Delta G^\circ)_{\text{ET Inter}}^d$		−0.25 eV	−0.31 eV	−0.27 eV
	$k_{\text{ET}} [\text{M}^{-1} \text{s}^{-1}]^e$		1.6×10^9	2.2×10^9	2.5×10^9
	$k_{\text{OXYGEN}} [\text{M}^{-1} \text{s}^{-1}]$		2.0×10^9	2.2×10^9	1.8×10^9
	$(\Delta G^\circ)_{\text{ET Intra}}^a$		−0.880 eV	−0.833 eV	−0.714 eV
	$\Phi_{\text{FLUORESCENCE}}$		0.24×10^{-4}	1.32×10^{-4}	1.92×10^{-4}
benzonitrile	$k_{\text{ET}} [\text{s}^{-1}]^b$		1.4×10^{10}	2.5×10^9	1.2×10^9
	τ_{singlet}		112 ps	289 ps	450 ps
	$k_{\text{ET}} [\text{s}^{-1}]^c$		8.9×10^9	3.5×10^9	2.2×10^9
	$k_{\text{BET}} [\text{s}^{-1}]^c$		6.9×10^8	5.4×10^8	5.1×10^8
	Φ_{TRIPLET}		0.88	0.96	0.97
	$(\Delta G^\circ)_{\text{ET Inter}}^d$		−0.669 eV	−0.729 eV	−0.689 eV
	$k_{\text{OXYGEN}} [\text{M}^{-1} \text{s}^{-1}]$		3.9×10^9	3.2×10^9	3.6×10^9
	$(\Delta G^\circ)_{\text{ET Intra}}^a$		−0.990 eV	−0.999 eV	−0.937 eV
	$\Phi_{\text{FLUORESCENCE}}$		0.12×10^{-4}	0.74×10^{-4}	0.98×10^{-4}
	$k_{\text{ET}} [\text{s}^{-1}]^b$		2.8×10^{10}	4.1×10^9	2.9×10^9
	τ_{SINGLET}		85 ps	184 ps	259 ps
	$k_{\text{ET}} [\text{s}^{-1}]^c$		1.2×10^{10}	5.4×10^9	3.9×10^9
$k_{\text{BET}} [\text{s}^{-1}]^c$		4.6×10^8	4.2×10^8	3.7×10^8	
Φ_{TRIPLET}		0.61	0.67	0.66	
$(\Delta G^\circ)_{\text{ET Inter}}^d$		−0.768 eV	−0.827 eV	−0.788 eV	
$k_{\text{ET}} [\text{M}^{-1} \text{s}^{-1}]^e$		7.0×10^8		9.1×10^8	
$k_{\text{OXYGEN}} [\text{M}^{-1} \text{s}^{-1}]$		3.1×10^9	3.0×10^9	3.0×10^9	

^a This determination was performed following the Continuum model: e.g., $\Delta G_{\text{ET}} = \Delta E_{0-0} - E_{\text{OX}} + E_{\text{RED}} - \Delta G_{\text{S}}$; $\Delta G_{\text{S}} = e^2/(4\Delta\epsilon_0) [(1/2R_+ + 1/2R_- - 1/R_{\text{D-A}}) 1/\epsilon_{\text{S}} - (1/2R_+ + 1/2R_-) 1/\epsilon_{\text{R}}]$; $E_{\text{OX}} = E_{1/2}(\text{TTF}/\text{TTF}^{+\cdot})$; $E_{\text{RED}} = E_{1/2}(\text{C}_{60}/\text{C}_{60}^{\cdot-})$; R_+ = radius TTF (7.6 Å); R_- = radius C_{60} (4.8 Å); ϵ_{S} = dielectric constant of solvent used for photophysical studies; ϵ_{R} = dielectric constant of solvent used for measuring the redox potential, namely, toluene:acetonitrile, 4:1 ($\epsilon_{\text{R}} = 9.24$); ΔE_{0-0} = excited-state energy of $^1\text{C}_{60}$ (1.762 eV). ^b Intramolecular electron transfer calculated from emission studies (eq 2) and assuming that the natural rate constants are the same as that of the reference compound. ^c Intramolecular electron and back electron transfer measured from picosecond experiments. ^d Determined as described in footnote a, but assuming 5 Å separation ($R_{\text{D-A}}$) and ΔE_{0-0} = excited-state energy of $^3\text{C}_{60}$ (1.50 eV). ^e Intermolecular electron transfer measured from nanosecond experiments. ^f τ_{ISC} measured from picosecond experiments.

$\sim 30^\circ$ in dyads **2a** and **7**. This distortion certainly impacts the coupling in these conjugated systems (**2a** and **7**) relative to **5** and, in turn, may slow the electron transfer.

Transient Spectroscopic Techniques: Intramolecular Electron-Transfer Event. The lower fluorescence quantum yields (i.e., the rapid deactivation of the photoexcited fullerene moieties) in dyads **2a**, **5**, and **7** relate to their effective engagement with the TTF centers. Pico- and nanosecond-resolved photolysis spectroscopic techniques are powerful means to characterize dynamic processes that are associated with the generation and fate of photoexcited states and, thus, complement the emission studies. With the scope to shed further light on the deactivation of the fullerene singlet excited-state, we probed these C_{60} –TTF dyads in transient flash photolysis following 18 ps 355 nm and 8 ns 337 nm laser pulses.

Picosecond photolysis of *N*-methyl fulleropyrrolidine (2.0×10^{-5} M) in oxygen-free toluene solutions leads to transient absorption changes revealing a maximum around 895 nm (Figure 4). Typically, this formation process is completed ~ 50 ps after the 355 nm laser excitation. These changes resemble the general observation for pristine C_{60} in toluene and are, accordingly, attributed to the singlet excited-state absorption ($^1\text{S}_1 \rightarrow ^1\text{S}_n$). Its decay follows clean first-order kinetics and results in the formation of the ($\text{T}_1 \rightarrow \text{T}_n$) absorption centered around

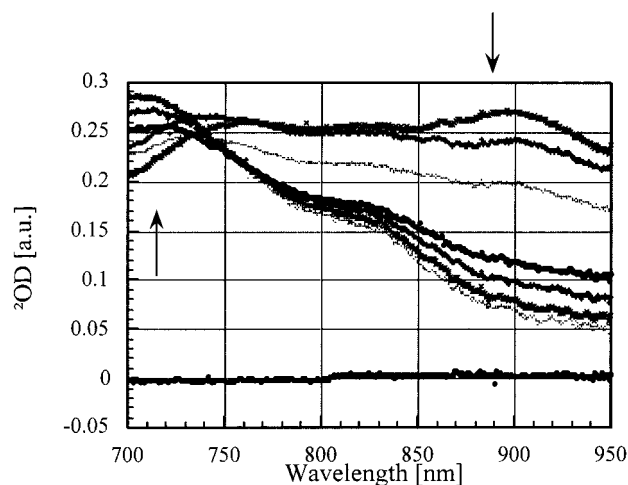


Figure 4. Time-resolved difference absorption spectra of excited singlet states and excited triplet states of *N*-methylfulleropyrrolidine (2.0×10^{-5} M) recorded 0, 50, 100, 500, 1000, 2000, 3000, and 4000 ps after excitation (355 nm) in oxygen-free toluene solution.

710 nm. It should be noted that for this fullerene reference, the associated singlet–triplet conversion (ISC) occurs with a rate (k_{ISC}) of $3.45 \times 10^8 \text{ s}^{-1}$.

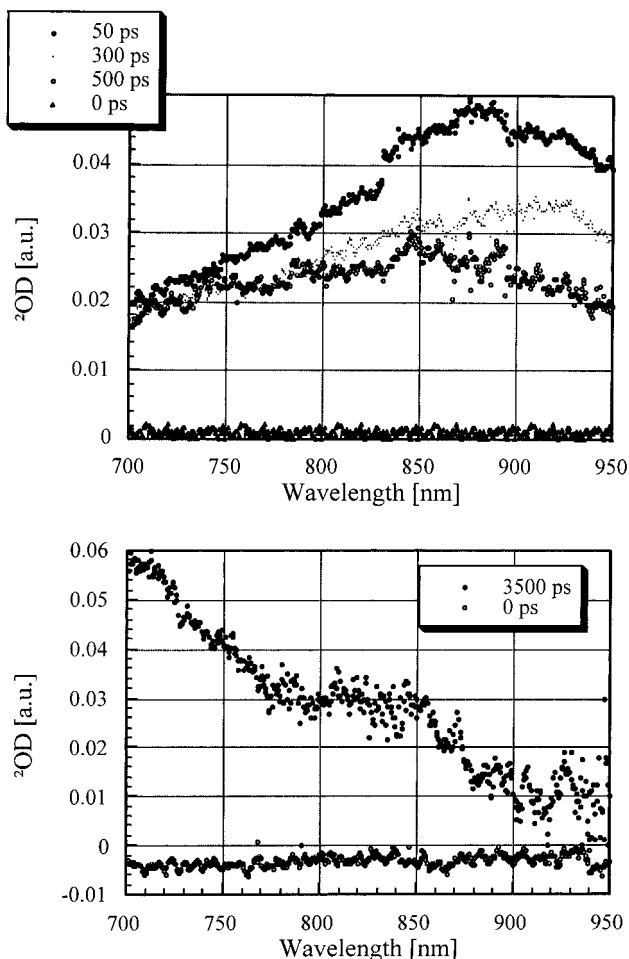


Figure 5. Time-resolved difference absorption spectra of excited singlet states and excited triplet states of dyad **5** (2.0×10^{-5} M) recorded (a) 0, 50, 300, and 500 ps after excitation (355 nm) and (b) 0 and 3500 ps after excitation in oxygen-free benzonitrile solution.

A similar formation of the fullerene singlet excited state ($\lambda_{\text{max}} = 890$ nm) is found in complementary picosecond experiments with dyads **2a**, **5**, and **7** in all investigated solvents (i.e., toluene, dichloromethane and benzonitrile; Figure 5a). The singlet lifetimes of the photoexcited fullerene core are significantly affected by the TTF moiety and also by the relative distance between the two redox-active sites. Specifically, in nonpolar toluene solutions, singlet lifetimes of 129, 395, and 680 ps were measured for dyads **2a**, **5**, and **7**, respectively. Furthermore, increasing the solvent polarity leads to a further shortening of the singlet lifetime for dyad **7**, for example. In conclusion, the distance and solvent dependence of the observed intramolecular rates resemble the results of the emission studies (see Table 2).

The transient absorption changes, typically recorded after the completion of the intramolecular transfer process, display no resemblance to the triplet excited state of *N*-methylfulleropyrrolidine; that is, the ($T_1 \rightarrow T_n$) absorption at 710 nm is clearly absent (see Figure 5; **5** in benzonitrile). Instead, the spectrum is characterized by a broad absorption (800–900 nm) that is similar to the one observed following intermolecular electron transfer (vide infra; Figure 7). Thus we tentatively ascribe this transient species to a charge-separated radical pair, namely, ($C_{60}^{\bullet-}$)-(TTF $^{\bullet+}$).

In general, the lifetime of the ($C_{60}^{\bullet-}$)-(TTF $^{\bullet+}$) pair in dyads **2a**, **5**, and **7** is very short. In dyad **5**, for example, back electron transfer rates (k_{BET}) of 6.89×10^8 and 4.59×10^8 s $^{-1}$ were measured in CH_2Cl_2 and benzonitrile, respectively. The short

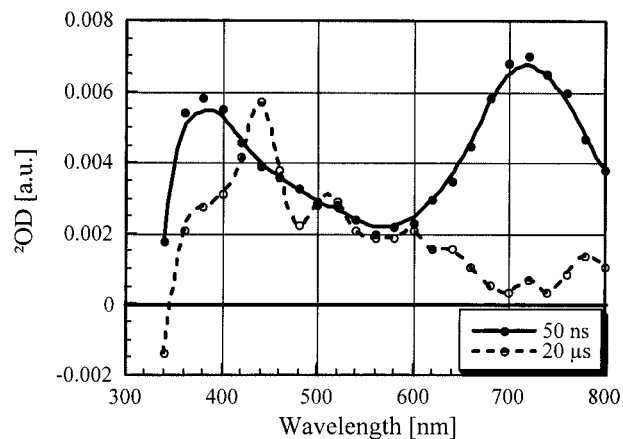
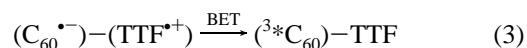


Figure 6. Transient absorption spectrum (UV-vis part) recorded 50 ns (●) and 20 μs (○) after flash photolysis of 2.0×10^{-5} M **5** at 337 nm in deoxygenated benzonitrile.

lifetime of the radical pair can be rationalized, at least in part, by the small spacer separating the electron-acceptor and electron-donor moieties in dyad **5**. In contrast, the larger spacers in dyads **2a** and **7** enhance the lifetime of ($C_{60}^{\bullet-}$)-(TTF $^{\bullet+}$), with rates (k_{BET}) ranging between 5.35×10^8 and 3.73×10^8 s $^{-1}$. The strong coupling induced by the π -conjugation in these rigidly spaced dyads (**2a** and **7**) undoubtedly mediates the fast back electron transfer (BET) in the latter two.

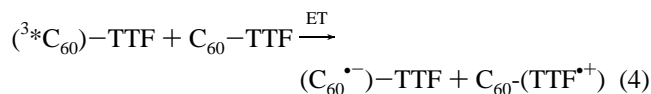
In all cases, the product of BET is the fullerene triplet excited-state characterized, as already mentioned, by a ($T_1 \rightarrow T_n$) absorption around 710 nm. The spectral assignment is further substantiated by the concurrent decay of the ($C_{60}^{\bullet-}$)-(TTF $^{\bullet+}$) radical pair absorption between 800 and 900 nm and the growing in of the ($^3C_{60}$)-TTF excited-state absorption at 710 nm (Figure 5b).



To illustrate the generation of the triplet excited state, Figure 6 depicts the differential absorption changes recorded for **5** (2.0×10^{-5} M) in oxygen-free benzonitrile solutions immediately (50 ns) after a 337 nm laser pulse. The set of two maxima at 380 and 710 nm is in close agreement with the triplet-triplet characteristics of earlier published spectra,³⁴ substantiating the generation of the triplet excited state. Probing a similar solution of the fullerene reference allowed the determination of the quantum yield of the fullerene triplet in dyads **2a**, **5**, and **7** via relative actinometry. Relative to the fullerene reference ($\Phi = 0.96$), the photoexcited dyads gave rise to similar triplet quantum yields in dichloromethane solutions ($\Phi = 0.88$ –0.97). In benzonitrile, however, the quantum yields were slightly lower ($\Phi = 0.61$ –0.87). The lower energy and longer lifetime of the ($C_{60}^{\bullet-}$)-(TTF $^{\bullet+}$) pair in benzonitrile solutions is a possible rationale for this difference.

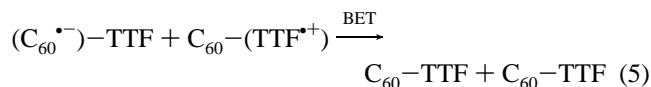
Intermolecular One-Electron Transfer. The triplet lifetimes of the fullerene core in dyads **2a**, **5**, and **7** exhibit a surprising dependence on the dyad concentration. In light of the oxidative power of the TTF addends, this observation suggests that the triplet excited state may be subject to an additional quenching reaction in addition to any triplet-triplet annihilation processes, namely, an intermolecular process. To support this hypothesis, we analyzed the differential absorption changes <20 μs after the laser pulse. Indeed, the 710 nm absorption band is absent in the visible region (Figure 6, 20 μs), but a new maximum around 440 nm and a set of weaker absorption bands at 510, 600, and 640 nm develop. The 440 nm peak, whose growth

matches the decay of the triplet absorption (710 nm), is in good agreement with the radiolytically generated TTF π -radical cation, namely, $\text{TTF}^{\bullet+}$ (see *Pulse Radiolysis*). More importantly, the spectral region between 750 and 1100 nm shows the time-resolved growth of a characteristic near-IR absorption band (Figure 7), whose formation match the accelerated decay of the 710 nm absorption. The identity of this band with the diagnostic peak of various fullerene π -radical anions³⁵ unquestionably confirms the formation of a charge-separated radical pair [e.g., $(\text{C}_{60}^{\bullet-})-(\text{TTF})/(\text{C}_{60}^{\bullet-})-(\text{TTF}^{\bullet+})$], evolving from a photoinduced electron transfer from the triplet and subsequent diffusional dissociation of the contact pair. (The absorption band around 810 nm helps to characterize the charge-separated radical pair on the picosecond time scale.)

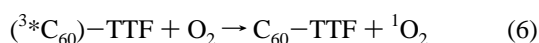


Enlarging the dyad (**2a**, **5**, and **7**) concentration and, therefore, quencher concentration, resulted in an increasingly faster deactivation of the triplet excited state. The applied dyad concentrations $[(1.0-0.05) \times 10^{-4} \text{ M}]$ gave rise to a linear dependence of the decay rate that, in turn, further supports a reductive quenching mechanism involving $({}^3\text{C}_{60})-\text{TTF}$. In benzonitrile, for example, an intermolecular quenching rate of $7 \times 10^8 \text{ M}^{-1} \text{ s}^{-1}$ was determined for **5**. A similar deactivation of the triplet excited state was noted in corresponding experiments in toluene and dichloromethane solutions. Stabilization of the radical pair is, however, largely hampered by the insufficient solvent polarity of these solvents. Accordingly, kinetic measurements in the concentration window $(1.0-0.05) \times 10^{-4} \text{ M}$ led to an accelerated decay of the triplet absorption, yielding the singlet ground state with a rate constant of $1.6 \times 10^9 \text{ M}^{-1} \text{ s}^{-1}$ in toluene. The excited-state behavior of dyads **2a** and **7** also follows this trend.

In benzonitrile solutions, the charge-separated radical pair is relatively stable and decays slowly over a few hundred microseconds, quantitatively yielding the singlet ground state. The lifetime of the $(\text{C}_{60}^{\bullet-})-\text{TTF}$ depends mainly on the dyad concentration $[(2.0-0.5) \times 10^{-5} \text{ M}]$. Specifically at high dyad concentrations that lead to a higher yield of charge-separated radicals, the lifetime is reduced. In fact, the decay of $(\text{C}_{60}^{\bullet-})-\text{TTF}$ (**5**) was found to be a second-order reaction, according to eq 5, with $k_2 = 3.9 \times 10^9 \text{ M}^{-1} \text{ s}^{-1}$.



In the presence of molecular oxygen, the electron-transfer route from the triplet state competes with an intermolecular energy transfer to generate singlet oxygen (${}^1\text{O}_2$) (eq 6). At dyad concentrations of $3.0 \times 10^{-5} \text{ M}$ (**5**), the fullerene triplet reacts with oxygen with rate constants of 2.0×10^9 , 3.9×10^9 , and $3.1 \times 10^9 \text{ M}^{-1} \text{ s}^{-1}$ in toluene, dichloromethane, and benzonitrile, respectively. It should be noted that similar rate constants were also derived for the fullerene reference and dyads **2a** and **7**.



Finally, in an attempt to confirm the absorption of the singly oxidized TTF moiety, pulse radiolytic oxidation experiments were carried out in oxygenated dichloromethane solutions. Radiolysis of this medium is known to provide the means for a selective one-electron oxidation process (see eq 7).³⁶ In

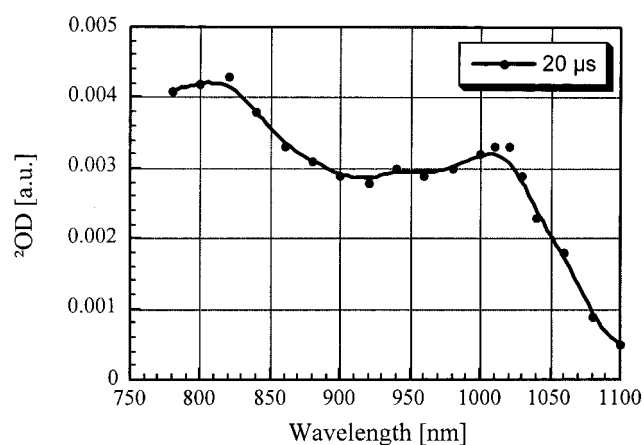


Figure 7. Transient absorption spectrum (near-IR part) recorded 20 μs (●) after flash photolysis of $2.0 \times 10^{-5} \text{ M}$ **5** at 337 nm in deoxygenated benzonitrile.

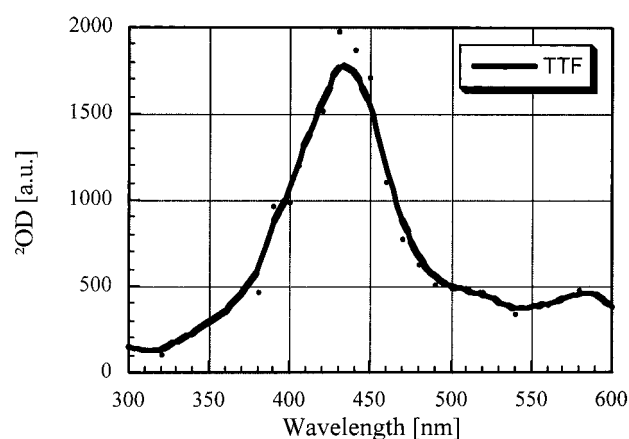


Figure 8. Transient absorption spectrum (UV-vis region) obtained after pulse radiolysis of TTF ($6.0 \times 10^{-5} \text{ M}$) in oxygenated dichloromethane solutions.

particular, pulse radiolysis of $5.0 \times 10^{-5} \text{ M}$ TTF in dichloromethane leads to differential absorption changes depicted in Figure 8. They disclose a pronounced maximum at 430 nm, similar to those seen in the nanosecond photolytic experiments (see Figure 6). Applying TTF at variable concentrations (e.g., ranging between 5.0×10^{-5} and $2.0 \times 10^{-3} \text{ M}$) resulted in an accelerated formation of the corresponding $(\text{TTF}^{\bullet+})$ absorption at 430 nm. The observed rate ($k_{\text{obs}} = \ln 2/\tau_{1/2}$) is linearly dependent on the TTF concentration, indicating that the underlying process is due to the following oxidation reaction (with a rate constant of $4.2 \times 10^8 \text{ M}^{-1} \text{ s}^{-1}$):

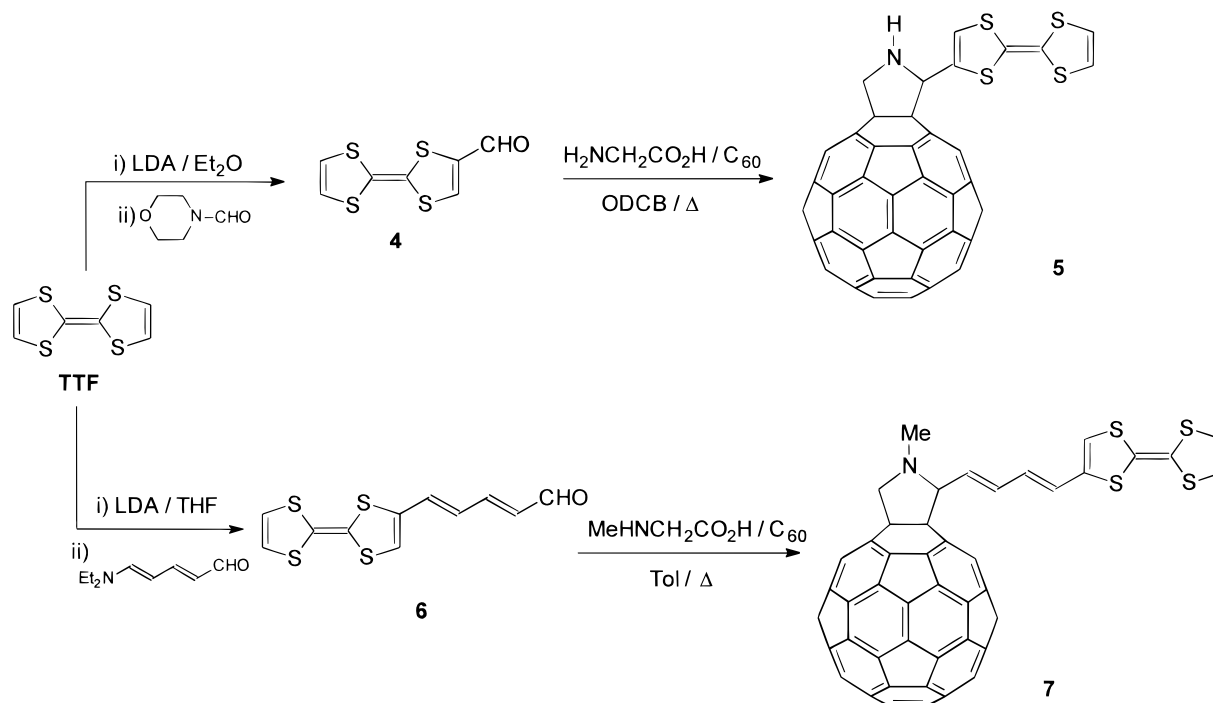


It should be noted that the initially formed solvent radical cation, $[\text{CH}_2\text{Cl}_2]^{\bullet+}$, despite being a powerful oxidant, does not engage with the TTF moiety on the monitored time-scale (up to 200 μs) because of the too short lifetime of $[\text{CH}_2\text{Cl}_2]^{\bullet+}$.

Summary and Conclusions

Novel C_{60} -based dyads, in which the C_{60} core is covalently linked to the electron donor tetrathiafulvalene (TTF), have been synthesized by 1,3-dipolar cycloadditions of in situ-generated TTF-containing azomethine ylides to C_{60} . Both donor and acceptor moieties are connected through a pyrrolidine ring (**5**) and one (**2a**) or two (**7**) additional vinyl groups. The electrochemical study of these dyads reveals, regardless of the spacer,

SCHEME 1



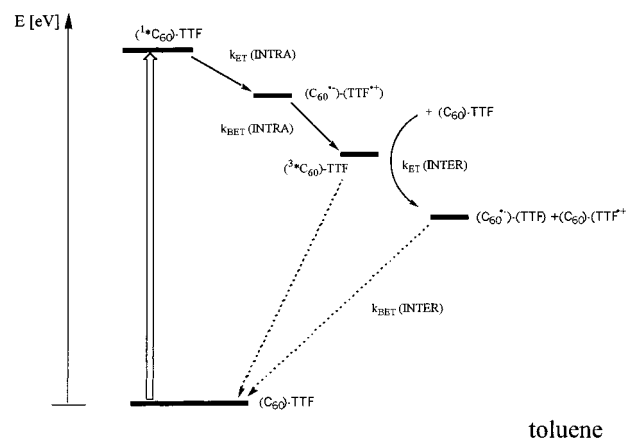
a very similar behavior. In general, all dyads show four reduction waves, corresponding to the first four reduction steps of the C_{60} core, and two oxidation waves at positive values, due to the formation of the radical cation and dication species of the TTF unit. Semiempirical calculations at the PM3 level show the spatial interchromophore distances and reveal a configuration in which the TTF fragment and the vinylogous spacers deviate from planarity but exhibit an energy similar to that calculated for the planar configuration.

Steady-state and time-resolved photolysis reveal that the fullerene singlet excited states in dyads **2a**, **5**, and **7** are subject to rapid intramolecular electron-transfer events yielding a short-lived charge-separated radical pair, namely, $(C_{60}^{\bullet-})-(TTF^{\bullet+})$. This result can be rationalized by the close distance of the donor-acceptor couple, for example in dyad **5**, or the strong coupling, induced by the vinylogous spacers in dyads **2a** and **7**. In contrast to fullerene-ferrocene and fullerene-aniline dyads, back electron transfer in **2a**, **5**, and **7** proceeds mainly via formation of the fullerene triplet excited state. The energy level of the latter (~ 1.50 eV) is still sufficient to activate a second, intermolecular electron transfer, as noticed earlier in bimolecular quenching between the triplet excited state of pristine C_{60} and TTF. Similarly, it is safe to assume that an intermolecular triplet quenching of the *N*-methyl fulleropyrrolidine (i.e., the fullerene core in dyads **2a**, **5**, and **7**) takes place; Scheme 2 illustrates this for dyad **2a** in toluene solutions.

In benzonitrile solutions, the energy level of the intramolecular radical pair in dyads **2a**, **5**, and **7** (~ 0.8 eV) falls, nevertheless, below that of the fullerene triplet excited state (1.50 eV). Despite the energetic argument, the nanosecond measurements provide unambiguous evidence for the fullerene triplet excited state, with lower quantum yields relative to that in toluene solutions.

One argument that could be forwarded is the energy of the intermolecular radical pair. In the context of stabilizing an intermolecular radical pair in reference to an intramolecular pair, the solvation energy of both species should be considered. In general, the free ions are better solvated than the intramolecular

SCHEME 2



radical pair. We are currently intensifying our work to calculate the solvation energies of the $(C_{60}^{\bullet-})-(TTF^{\bullet+})$ and $(C_{60}^{\bullet-})/(TTF^{\bullet+})$ pairs more precisely. A more likely reason for this surprising observation may arise from an electron-transfer process in the singlet excited state that proceeds with an efficiency less than unity.

Experimental Section

General Details. The 1H NMR and ^{13}C NMR spectra were obtained with a Varian VXR 300. Mass spectra were recorded with a VC Autospec EBE spectrometer operating at 30 kV, using a bombardment of Cs^+ ions and 2-nitrophenyloctyl ether (2-NPOE) or 3-NBA as matrix. The FTIR spectra were recorded with a Nicolet Magna-IR spectrometer 5550. Cyclic voltammetry measurements were performed on an EG&G PAR Versastat potentiostat using 250 Electrochemical Analysis software. A Metrohm 6.0804.C10 glassy carbon electrode was used as indicator electrode in voltammetric studies 1×10^{-5} M solutions of the compound in dichloromethane, 0.1 M Bu_4NClO_4 as the supporting electrolyte; platinum working and

counter electrode; saturated calomel electrode (SCE) as reference electrode at 20 °C. All chromatography was performed with Merck silica gel (70–230 mesh). All reagents were used as purchased unless otherwise stated. All solvents were dried according to standard procedures. All reactions were carried out under an atmosphere of dry argon.

Semiempirical calculations were carried out at the PM3/RHF level with the Hyperchem 5.1 program package.³¹

Picosecond laser flash photolysis experiments were carried out with 355-nm laser pulses from a mode-locked, Q-switched Quantel YG-501 DP ND:YAG laser system (pulse width ~18 ps, 2–3 mJ/pulse). The white continuum picosecond probe pulse was generated by passing the fundamental output through a D₂O/H₂O solution. Nanosecond laser flash photolysis experiments were performed with laser pulses from a Moletron UV-400 nitrogen laser system (337.1 nm, 8 ns pulse width, 1 mJ/pulse) in a front-face excitation geometry. The photomultiplier output was digitized with a Tektronix 7912 AD programmable digitizer.³⁸ Pulse radiolysis experiments were accomplished with 50 ns pulses of 8 MeV electrons from a model TB-8/16-1S electron linear accelerator. Dosimetry was based on the oxidation of SCN⁻ to (SCN)₂^{•-}, which, in N₂O-saturated aqueous solutions, takes place with $G \sim 6$ (G denotes the number of species per 100 eV, or the approximate micromolar concentration per 10 J of absorbed energy). The radical concentration generated per pulse amounts to $(1-3) \times 10^{-6}$ M for all systems investigated in this study.³⁹ Absorption spectra were recorded with a Milton Roy Spectronic 3000 Array spectrophotometer. Emission spectra were recorded on a SLM 8100 Spectrofluorimeter.

N-Methyl-2'-[2-(tetrathiafulvalenyl)ethenyl]pyrrolidino[3',4':1,2][60]fullerene (2a). This compound was synthesized by following the previously reported procedure.^{20,28}

2'-(Tetrathiafulvalenyl)pyrrolidino[3',4':1,2][60]fullerene (5). An ODCB solution of C₆₀ (100 mg, 0.138 mmol), formyl-TTF (4) (64.8 mg, 0.277 mmol), and glycine (20.85 mg, 6.277 mmol) was heated to reflux under argon atmosphere for 2 h. The solvent was removed under reduced pressure, and the crude material was carefully chromatographed on a silica gel column using cyclohexane and a cyclohexane:toluene (1:1) mixture as eluent. Further purification was accomplished by repetitive precipitation and centrifugation using methanol as solvent. 30% yield (43% based on recovered C₆₀); ¹H NMR (300 MHz, CDCl₃/CS₂ 1/1) δ : 6.73 (1H, s), 6.31 (2H, s), 5.63 (1H, s), 5.01 (1H, d, $J = 10.2$), 4.77 (1H, d, $J = 10.2$); ¹³C NMR (75 MHz, CDCl₃/CS₂ 1/1) δ : 155.0, 153.5, 152.4, 151.5, 148.0, 147.1, 146.8, 146.1, 146.0, 145.9, 145.8, 145.5, 145.4, 145.3, 145.1, 144.5, 142.5, 142.1, 141.8, 141.5, 134.7, 119.1, 118.9, 117.5, 117.4, 77.2, 72.7, 71.4, 61.0; FTIR (KBr): 2850, 1736, 1494, 1462, 1261, 1081, 966, 795, 753, 640, 526 cm⁻¹; UV-vis (CH₂Cl₂) λ_{\max} (log ϵ): 232 (4.86), 258 (5.01), 316 (4.63), 430 (3.72) nm; MS (FAB⁺) (m/z): 965 (M⁺, 23%), 720 (58%).

N-Methyl-2'-[4-(tetrathiafulvalenyl)butadienyl]pyrrolidino[3',4':1,2][60]fullerene (7). A toluene solution of C₆₀ (200 mg, 0.33 mmol), TTF derivative (6) (80 mg, 0.28 mmol), and sarcosine (20.85 mg, 6.277 mmol) was heated to reflux for 24 h. The solvent was removed under reduced pressure, and the crude material was carefully chromatographed on a silica gel column with a cyclohexane:toluene (1:1) mixture as eluent. Further purification was accomplished by repetitive precipitation and centrifugation: 27% yield (53% based on recovered C₆₀); ¹H NMR (300 MHz, CDCl₃/CS₂ 1/1) δ : 7.21 (1H, d, $J = 6.9$), 7.13 (1H, d, $J = 6.9$), 6.72 (1H, dd, $J_1 = 15.3$, $J_2 = 10.2$), 6.43

(1H, d, $J = 15.3$), 6.28 (3H, m), 4.85 (1H, d, $J = 9.3$), 4.38 (1H, d, $J = 8.7$), 4.12 (1H, d, $J = 9.3$), 2.87 (3H, s); ¹³C NMR (75 MHz, CDCl₃/CS₂ 1/1) δ 147.2, 146.7, 146.3, 146.2, 146.0, 145.2, 145.1, 145.0, 144.6, 144.3, 144.1, 143.1, 142.6, 142.5, 142.1, 142.0, 140.2, 136.3, 135.5, 135.1, 133.5, 132.7, 130.6, 128.9, 128.1, 125.4, 125.2, 125.0, 123.9, 120.8, 119.5, 119.0, 118.9, 118.6, 111.2, 110.6, 81.8, 77.2, 69.7, 69.3, 40.1; FTIR (KBr) 1634, 1462, 1330, 1230, 180, 1027, 976, 795, 767, 729, 639, 598, 574, 562, 553, 526 cm⁻¹; UV-vis (CH₂Cl₂) λ_{\max} (log ϵ): 232 (3.97), 258 (5.20), 318 (1.83), 432 (0.97) nm; MS (FAB⁺) (m/z): 1031 (M⁺, 19%), 720 (98%).

Acknowledgment. We are indebted to DGICYT (Project PB95-0428-CO2) for financial support. M.A.H. acknowledges M.E.C. of Spain for a research fellowship. Some of this work was supported by the Office of Basic Energy Sciences of the U.S. Department of Energy (contribution no. NDR-4107) from the Notre Dame Radiation Laboratory). We thank Dr. G. Hug for many helpful discussions and Dr. I. Carmichael for the PM3 calculations of the TTF HOMO and LUMO.

References and Notes

- Wasielowski, M. R. in *Photoinduced Electron Transfer*, Fox, M. A.; Chanon, M., Eds.; Elsevier: Amsterdam, 1988.
- Wasielowski, M. R. *Chem. Rev.* **1992**, *92*, 435.
- Gust, D.; Moore, T. A.; Moore, A. L. *Acc. Chem. Res.* **1993**, *26*, 198.
- Paddon-Row, M. N. *Acc. Chem. Res.* **1994**, *27*, 18.
- Kurreck, H.; Huber, M. *Angew. Chem., Int. Ed. Engl.* **1995**, *34*, 849.
- Kroto, H. W.; Heath, J. R.; O'Brien, S. C.; Curl, R. F.; Smalley, R. E. *Nature* **1985**, *318*, 162.
- Krättsmer, W.; Lamb, L. D.; Fostiropoulos, K.; Huffman, D. R. *Nature* **1990**, *347*, 354.
- Sun, Y.-P. In *Molecular and Supramolecular Photochemistry*; Ramamurthy, V.; Schanze, K., Eds.; Marcel Dekker: New York, 1997; Vol. 1. Prato, M. *J. Mater. Chem.* **1997**, *7*, 1097. Imahori, H.; Sakata, Y. *Adv. Mater.* **1997**, *9*, 537.
- Williams, R. M.; Koeberg, M.; Lawson, J. M.; An, Y.-Z.; Rubin, Y.; Paddon-Row, M. N.; Verhoeven, J. W. *J. Org. Chem.* **1996**, *61*, 5055.
- Guldi, D. M.; Asmus, K.-D. *J. Am. Chem. Soc.* **1997**, *119*, 5744. Imahori, H.; Hagiwara, K.; Akiyama, T.; Aoki, M.; Taniguchi, S.; Okada, T.; Shirakawa, M.; Sakata, Y. *Chem. Phys. Lett.* **1996**, *263*, 545.
- For a very recent review on C₆₀-based electroactive organofullerenes, see: Martín, N.; Sánchez, L.; Illescas, B.; Pérez, I. *Chem. Rev.* **1998**, *98*, 2527.
- Prato, M.; Maggini, M. *Acc. Chem. Res.* **1998**, *31*, 519. Diederich, F.; Thilgen, C. *Science* **1996**, *271*, 317. Taylor, R.; Walton, D. R. M. *Nature* **1993**, *363*, 685.
- For a recent review on addition reactions of Buckminsterfullerene-C₆₀, see: Hirsch, A. *Synthesis* **1995**, 895. Diels-Alder reactions were systematically introduced into fullerene chemistry by Rubin and Müllen; see: Rubin, Y.; Khan, S.; Freedberg, D. I.; Yerezian, C. *J. Am. Chem. Soc.* **1993**, *115*, 344. Belik, P.; Gügel, A.; Spickermann, J.; Müllen, K. *Angew. Chem., Int. Ed. Engl.* **1993**, *32*, 78. Gügel, A.; Kraus, A.; Spickermann, J.; Belik, P.; Müllen, K. *Angew. Chem., Int. Ed. Engl.* **1994**, *33*, 559. For recent examples of 1,3-dipolar cycloadditions to C₆₀ see: *Tetrahedron* **1996**, *52*, 4925–5262 (special issue on "Fullerene Chemistry", Smith, A. B., III, Ed.).
- Bingel, C. *Chem. Ber.* **1993**, *126*, 1957.
- Bryce, M. R. *J. Mater. Chem.* **1995**, *5*, 1481. See also: *Handbook of Organic Conductive Molecules and Polymers*; Nalwa, N. S., Ed.; John Wiley & Sons: New York, 1997; Vol. 1.
- González, M.; Martín, N.; Segura, J. L.; Garín, J.; Orduna, J. *Tetrahedron Lett.* **1998**, *39*, 3269.
- Becher, J. *Synthesis* **1980**, 589.
- Jutz, C. *Chem. Ber.* **1958**, *91*, 1867.
- Friedly, A. C.; Yang, E.; Marder, S. R. *Tetrahedron* **1997**, *53*, 2717.
- Martín, N.; Sánchez, L.; Seoane, C.; Andreu, R.; Garín, J.; Orduna, J. *Tetrahedron Lett.* **1996**, *37*, 5979.
- Prato, M.; Maggini, M.; Giacometti, C.; Scorrano, G.; Sandoná, G.; Farnia, G. *Tetrahedron* **1996**, *52*, 5221.
- Hudhomme, P.; Boullé, C.; Rabreau, J. M.; Cariou, M.; Jubault, M.; Gorgues, A. *Synth. Met.* **1998**, *94*, 73. Boullé, C.; Rabreau, J. M.; Hudhomme, P.; Cariou, M.; Jubault, M.; Gorgues, A.; Orduna, J.; Garín, J.

Tetrahedron Lett. **1997**, 38, 3909. Llacay, J.; Mas, M.; Molins, E.; Veciana, J.; Powell, D.; Rovira, C. *Chem. Commun.* **1997**, 659.

(23) Llacay, J.; Veciana, J.; Vidal-Gancedo, J.; Bourdelande, J. L.; González-Moreno, R.; Rovira, C. *J. Org. Chem.* **1998**, 63, 5201.

(24) Balzani, V. In *Supramolecular Photochemistry*; D. Reidel: Dordrecht, The Netherlands, 1987. Gust, D.; Moore, T. A. *Photoinduced Electron Transfer*; Mattay, J., Ed.; Springer: Berlin, 1991; Vol. III. Carter, F. L. *Molecular Electronic Devices*; Marcel Dekker: New York, 1987.

(25) Maggini, M.; Scorrano, G.; Prato, M. *J. Am. Chem. Soc.* **1993**, 115, 9798.

(26) Green, D. C. *J. Org. Chem.* **1979**, 44, 1476. Garín, J.; Orduna, J.; Uriel, S.; Moore, A. J.; Bryce, M. R.; Wegener, S.; Yufit, D. S.; Howard, J. A. K. *Synthesis* **1994**, 489.

(27) Maggini, M.; Karlsson, A.; Scorrano, G.; Sardoná, G.; Farnia, G.; Prato, M. *J. Chem. Soc., Chem. Commun.* **1994**, 589.

(28) Martín, N.; Sánchez, L.; Seoane, C.; Andreu, R.; Garín, J.; Orduna, J.; Ortí, E.; Viruela, P. M.; Viruela, R. *J. Phys. Chem. Solids* **1997**, 58, 1713.

(29) Suzuki, T.; Maruyama, Y.; Akasaba, T.; Ando, W.; Kobayashi, K.; Nagase, S. *J. Am. Chem. Soc.* **1994**, 116, 1359. Chlistouff, J.; Clifffel, D.; Bard, A. J. In *Handbook of Organic Conductive Molecules and Polymer*; Nalwa, N. S., Ed.; John Wiley & Sons: New York; 1997, Vol. 1, Ch. 7. Echegoyen, L.; Echegoyen, L. E. *Acc. Chem. Res.* **1998**, 31, 593.

(30) Khodorkovsky, V.; Becker, J. I. In *Organic Conductors: Fundamentals and Applications*; Farges, J.-P., Ed.; Marcel Dekker: New York, 1994; Chapter 3.

(31) HyperChem 5.1, Hypercube, Inc., Waterloo, Ontario N2L 2 × 2, Canada, 1997.

(32) Guldi, D. M.; Maggini, M.; Scorrano, G.; Prato, M. *J. Am. Chem. Soc.* **1997**, 119, 974. Williams, R. M.; Zwier, J. M.; Verhoeven, J. W. *J. Am. Chem. Soc.* **1995**, 117, 4093.

(33) Imahori, H.; Hagiwara, K.; Aoki, M.; Akiyama, T.; Taniguchi, S.; Okada, T.; Shirakawa, M.; Sakata, Y. *J. Am. Chem. Soc.* **1996**, 118, 11 771.

(34) Guldi, D. M.; Asmus, K.-D. *J. Phys. Chem. A* **1997**, 101, 1472.

(35) Kato, T.; Kodama, T.; Shida, T.; Nakagawa, T.; Matsui, Y.; Suzuki, S.; Shiromaru, H.; Yamauchi, K.; Achiba, Y. *Chem. Phys. Lett.* **1991**, 180, 446. Guldi, D. M.; Hungerbühler, H.; Janata, E.; Asmus, K.-D. *J. Phys. Chem.* **1993**, 97, 11 258.

(36) Guldi, D. M.; Neta, P.; Hambright, P. *J. Chem. Soc., Faraday Trans.* **1992**, 88, 2013.

(37) Maciejewski, A.; Steer, R. P. *Chem. Rev.* **1993**, 93, 67.

(38) Ebbesen, T. W. *Rev. Sci. Instrum.* **1988**, 59, 1307. Nagarajan, V.; Fessenden, R. W. *J. Phys. Chem.* **1985**, 89, 2330.

(39) Asmus, K.-D. *Methods Enzymol.* **1984**, 105, 167.